Passband reconstruction from photometry

Michael Weiler, Carme Jordi, Josep Manel Carrasco and Claus Fabricius

Institut de Ciències del Cosmos, Universitat de Barcelona, Spain
email: mweiler@fqa.ub.edu

Abstract. Photometric passbands are usually characterised through laboratory measurements and once in operations they are refined with true observations of reference sources with known spectral energy distribution. This paper revises the methods to determine those passbands and discusses the limitations encountered. The passbands are not fully constrained by the reference sources used and the method presented here allows to evaluate which is the constrained and the unconstrained component of the passband.

Keywords. standards, techniques: photometric, methods: analytical

1. Introduction

The interpretation of photometric observations in astrophysical terms requires knowledge of the photometric passbands the observations were performed in. These passbands are usually pre-defined by simulations and laboratory measurements on individual components of instrumentation, such as filter transmissivities and mirror reflectances. Once in operation, the passbands are refined using actual observations of astronomical objects with know spectral energy distributions. Weiler *et al.* (2018) have presented a detailed analysis of the constraints inherent to any reconstruction of the passband from photometric observations. In this work we summarise the important findings, provide a graphical interpretation of the results, and present examples for the reconstruction of the passband of ESA's HIPPARCOS mission ESA (1997).

2. Theoretical framework

2.1. *The mathematical formalism*

We consider the problem, that for a set of N calibration sources we have known spectral photon distributions (SPDs), as well as photometric observations in some passband. We want to determine the passband, i.e. derive the wavelength-dependent response curve $p(\lambda)$, λ being the wavelength. We assume $p(\lambda)$ to be the "photon response curve", i.e. the ratio of recorded photons (or, photo electrons) over the total number of photons entering the instrument. If c_i denotes the recorded number of photons per unit of time and aperture area for the calibration source i, $i = 1, \ldots, N$, and $s_i(\lambda)$ the SPD of that source in terms of photons per unit of time, wavelength, and aperture area, then these two quantities are linked by the response curve via

$$c_i = \int\limits_{\lambda_0}^{\lambda_1} p(\lambda) \cdot s_i(\lambda) \, \mathrm{d}\lambda. \tag{2.1}$$

This integral is evaluated over a finite wavelength interval $I = [\lambda_0, \lambda_1]$ which is chosen such that we can a-priori assume the response curve to be identical to zero everywhere outside I. To derive a suitable mathematical formalism in this context, we make use of

472

the fact that both functions, $p(\lambda)$ and $s_i(\lambda)$, are for physical reasons square-integrable, i.e. the integral ofter the square of each of the functions has to be finite. All square integrable functions on the interval I form a vector space over the field of real numbers, which is endowed with a conical scalar product defined by

$$\langle\, f_1 \mid f_2 \,\rangle := \int\limits_{\lambda_0}^{\lambda_2} f_1(\lambda) \cdot f_2(\lambda)\, \mathrm{d}\lambda. \tag{2.2}$$

Thanks to the scalar product, this vector space of square integrable functions on the interval I, denoted $\mathcal{L}^2(I)$, has properties which widely correspond to the properties well familiar from the more graphic Euclidian vector spaces. Elements of $\mathcal{L}^2$ can be developed in bases, and the existence of the scalar product ensures that bases can be chosen orthonormal. The scalar product also introduces a norm measuring the lengths of vectors, a metric measuring the distances between vectors, and angles between vectors. When we want to emphasise the vector nature of a function $f(\lambda)$ on the interval I, we conventionally write $|f\rangle$ for it. This convention corresponds to the convention of putting a little arrow on top of a letter to emphasise the vector nature of the corresponding quantity in a Euclidian vector space. Table 1 provides an overview of the correspondences between the well familiar Euclidian spaces and vector spaces formed by square-integrable functions.

Such a vector-based approach has first been introduced in photometry by Young (1994) for the problem of photometric transformations. Using this formalism also for the problem of passband reconstruction, we can write in short for Eq. (2.1)

$$c_i = \langle\, s_i \mid p \,\rangle \quad, i = 1, \ldots, N \tag{2.3}$$

and develop the N SPDs $|s_i\rangle$ in M orthonormal basis functions $|\varphi_j\rangle$, $j = 1, \ldots, M$ and $1 \leq M \leq N$,

$$|s_i\rangle = \sum_{j=1}^{M} a_{ij}\, |\varphi_j\rangle. \tag{2.4}$$

Taking $\mathbf{A}$ as the $N \times M$ matrix containing the coefficients a_{ij} of the development of the ith calibration SPD in the jth basis function, and combine the photometric observations c_i in a N–vector $\mathbf{c}$, we obtain

$$\mathbf{c} = \mathbf{A}\, \mathbf{p}_\parallel, \tag{2.5}$$

with $\mathbf{p}_\parallel$ the M–vector whose $j-$th element is

$$p_j = \langle\, p \mid \varphi_j \,\rangle. \tag{2.6}$$

Thus, $\mathbf{p}_\parallel$ is the vector containing the coefficients of the passband $|p\rangle$ developed in the basis $\{|\varphi_j\rangle\}_{j=1,\ldots,M}$. The optimal solution for the response curve $p(\lambda)$ can therefore be obtained by solving the simple linear system of equations that is Eq. (2.5) for $\mathbf{p}_\parallel$. Two observations are of importance in this respect.

First, in Eq. (2.4) we developed the N calibration SPDs $|s_i\rangle$ in a M–dimensional basis, with $1 \leq M \leq N$. Such a basis arises naturally from a set of N given vectors which contain M linearly independent vectors, where M is at least one and cannot exceed the number of vectors N. The optimal choice for the basis $\{|\varphi_j\rangle\}_{j=1,\ldots,M}$ is therefore derived from the calibration SPDs themselves. One may select the M linear independent vectors among the N vectors $|s_i\rangle$ and orthonormalize them. In practice, where the calibration SPDs may be available in tabulated form, this step can easily be done by a functional principal component analysis.

Second, the solution of Eq. (2.5) does not uniquely determine the passband. In fact, the solution for $\mathbf{p}_\parallel$ only provides the projection of the passband $|p\rangle$ onto the sub-space

Table 1. Comparison between Euclidian vector spaces and $\mathcal{L}^2$ over the field of real numbers.

Object	$\mathbb{R}^n$	$\mathcal{L}^2$
Notation for vector and basis vector	$\vec{r}$ and $\vec{e}_i$	$|f\rangle$ and $|\varphi_i\rangle$
Basis development	$\vec{r} = \sum_{i=1}^{n} a_i\,\vec{e}_i\,,\,a_i \in \mathbb{R}$	$|f\rangle = \sum_{i=0}^{\infty} a_i\,|\varphi_i\rangle\,,\,a_i \in \mathbb{R}$
Scalar product	$\vec{r}_1 \cdot \vec{r}_2$	$\langle\,f_1\,|\,f_2\,\rangle$
Orthonormality of basis	$\vec{e}_i \cdot \vec{e}_j = \delta_{ij}$	$\langle\,\varphi_i\,|\,\varphi_j\,\rangle = \delta_{ij}$
Projection onto a basis vector	$(\vec{r} \cdot \vec{e}_i) \cdot \vec{e}_i\,[= a_i\,\vec{e}_i]$	$\langle\,f\,|\,\varphi_i\,\rangle \cdot |\varphi_i\rangle\,[= a_i\,|\varphi_i\rangle]$
Norm ("Length")	$\sqrt{\vec{r} \cdot \vec{r}}$	$\sqrt{\langle\,f\,|\,f\,\rangle}$
Metric ("Distance")	$\sqrt{(\vec{r}_1 - \vec{r}_2) \cdot (\vec{r}_1 - \vec{r}_2)}$	$\sqrt{\langle\,f_1 - f_2\,|\,f_1 - f_2\,\rangle}$
Angle	$\mathrm{acos}\left(\frac{\vec{r}_1 \cdot \vec{r}_2}{\sqrt{\vec{r}_1 \cdot \vec{r}_1}\,\sqrt{\vec{r}_2 \cdot \vec{r}_2}}\right)$	$\mathrm{acos}\left(\frac{\langle\,f_1\,|\,f_2\,\rangle}{\sqrt{\langle\,f_1\,|\,f_1\,\rangle\,\langle\,f_2\,|\,f_2\,\rangle}}\right)$

of $\mathcal{L}^2(I)$ that is spanned by the calibration SPDs. This will in general be a poor approximation to $|p\rangle$. We may however add any vector $|p_\perp\rangle$ which is orthogonal to the sub-space spanned by the SPDs, i.e. which is satisfying the conditions

$$\langle\,p_\perp\,|\,\varphi_j\,\rangle = 0 \quad,\, j = 1, \ldots, M, \tag{2.7}$$

to our solution $|p_\parallel\rangle$ without affecting the synthetic photometry of the calibration sources. We therefore write

$$|p\rangle = |p_\parallel\rangle + |p_\perp\rangle. \tag{2.8}$$

The component $|p_\parallel\rangle$ in this sum we refer to as the "parallel component" of the passband (with respect to the set of calibration sources used in the passband determination). This component is uniquely determined by the set of calibration SPDs available for passband determination and can be easily found by solving Eq. (2.5). The second component of the passband, $|p_\perp\rangle$, we refer to as the "orthogonal component". This component is entirely unconstrained by the set of calibration SPDs. We have to estimate this component, in such a way that the resulting passband $|p\rangle$ is satisfying the physical constraints (i.e., being non-negative, bound to unity in case of non-amplifying photon detectors) and in reasonable agreement with the available a-priori knowledge about the general shape of the passband.

The fact that the passband contains a component that is not constrained by the calibration SPDs may have important consequences for the synthetic photometry of SPDs which depend on the unconstrained orthogonal passband component. The need for eventually guessing $|p_\perp\rangle$ introduces a fundamental uncertainty to the passband $|p\rangle$. While for SPDs which lay within the sub-space of $\mathcal{L}^2(I)$ spanned by the calibration SPDs, i.e. which can be well described as a linear combination of the calibration SPDs, the synthetic photometry is reliable and unaffected by uncertainties in $|p_\perp\rangle$, this is not the case for SPDs that fall significantly out of this sub-space. For the later SPDs the uncertainty in $|p_\perp\rangle$ may introduce systematic errors in the synthetic photometry.

As contributions from $|p_\perp\rangle$, and the associated uncertainty, cannot be excluded in general, one may use the two passband components individually when computing the synthetic photometry for some SPD of interest. The ratio of the contributions of the two passband components to synthetic photometry, $\langle\,s\,|\,p_\perp\,\rangle / \langle\,s\,|\,p_\parallel\,\rangle$, then provides an estimate on how sensitive the photometric photometry is to the unconstrained component. A more graphical measure for this sensitivity is obtained if the ratio is weighted by the norms of

the passband components, and converted into an angle by taking the inverse tangent,

$$\gamma = \text{atan} \left(\frac{\langle s \,|\, p_\perp \rangle}{\langle s \,|\, p_\| \rangle} \sqrt{\frac{\langle p_\| \,|p_\| \rangle}{\langle p_\perp \,|p_\perp \rangle}} \right). \tag{2.9}$$

This angle γ gives the orientation of some SPD $|s\rangle$ with respect to $|p_\|\rangle$, measured in the plane spanned by the two components $|p_\|\rangle$ and $|p_\perp\rangle$.

2.2. *Graphical interpretation*

The close analogy between Euclidian vector spaces and vector spaces of square integrable functions, as highlighted in Table 1, allows for a graphical illustration of the formalism described so far. For a truly graphical interpretation it is of course necessary to reduce the dimensionality of the problem. We replace the infinite-dimensional space of functions by a three-dimensional space, and we set $M = 1$, which corresponds to a situation where only calibration spectra of a single shape are available. In this case, the sub-space spanned by the calibration spectra is one-dimensional, which is graphically to be interpreted as a line. This case is shown in the left-hand panel of Fig. 1. The axes of the three-dimensional space are chosen arbitrarily in this figure, i.e. without any specific orientation with respect to the vectors of interest. The ($M = 1$)-dimensional sub-space spanned by the calibration SPDs is illustrated as a black line. The parallel component of the passband, shown as a red arrow, is oriented along this line. In a three-dimensional space, the orthogonal space to the one-dimensional line is a two-dimensional plane, oriented perpendicular to the line. The orientation of this plane is indicated by the blue circle. Any vector inside that plane can be added to $|p_\|\rangle$ without affecting the synthetic photometry for the calibration sources. The component of the passband within this plane is therefore unconstrained. Choosing the length and orientation of a vector within the plane for the orthogonal component of the passband has to be done such that the sum of the parallel and orthogonal component is in a position in agreement with the a-priori knowledge on the passband. This sum, the actual assumption of the passband, is shown as a green arrow in Fig. 1. The green shaded region indicates the plane spanned by the parallel and orthogonal component of the passband, being perpendicular to the blue plane of the orthogonal space.

The right-hand panel in Fig. 1 illustrates the situation when computing synthetic photometry. A SPD $|s\rangle$, shown as a magenta arrow, may lay somewhere in space. The contributions of the parallel and orthogonal components of the passband to the synthetic photometry for that SPD depend on the projections of $|s\rangle$ onto these passband components. These are shown as the orange on cyan lines, respectively. As the vector of the parallel component is constrained by the calibration sources, so is the projection of the SPD onto it. The projection onto the orthogonal component depends on the choice made for $|p_\perp\rangle$, illustrating the uncertainty in the synthetic photometry resulting from the orthogonal component. The dashed magenta line shows the projection of the SPD onto the plane spanned by the parallel and orthogonal passband components. The angle γ lays in this plane and is indicated in green. It measures from $|p_\|\rangle$ towards $|p_\perp\rangle$ and serves as a measure for the dependency of the synthetic photometry on the choice of $|p_\perp\rangle$. A value of zero for γ corresponds to a case where the projection of the SPD onto the plane spanned by $|p_\|\rangle$ and $|p_\perp\rangle$ coincides with the parallel component, and the synthetic photometry thus being independent of the selected orthogonal component. This situation corresponds to a reliable result for the synthetic magnitude. For $\gamma = 90°$, the opposite occurs. The synthetic photometry solely depends on the choice for $|p_\perp\rangle$, which may result in considerable systematic uncertainties on the synthetic magnitudes.
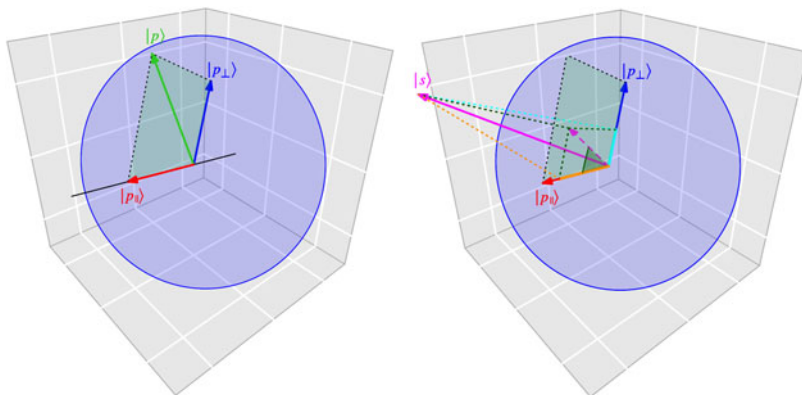
Figure 1. Sketch of the formalism described in this work. Left: Decomposition of the passband into parallel and orthogonal component. Right: Decomposition of a SPD with respect to the parallel and orthogonal passband components. For details see text.

2.3. *Estimating the orthogonal component*

The orthogonal passband component $|p_\perp\rangle$ has to be estimated such that its sum with $|p_\parallel\rangle$ satisfies the conditions one can a-priori impose on the passband, such as being non-negative and smooth. In particular the requirement for smoothness can be difficult to meet. The parallel component is determined by the shape of the calibration spectra, which are expected to contain many spectral features on many different scales. In order to easily find an orthogonal component compensating these features, it may be convenient to start from a smooth initial guess for the passband, $|p_{ini}\rangle$. One then may define a simple model for modifying the initial guess in a smooth way, and imposing the resulting modification to meet the parallel component derived by solving Eq. (2.5). We thus express the passband by a model

$$|p\rangle = \left(\sum_{k=0}^{K-1} \alpha_k \cdot \phi_k(\lambda) \right) |p_{ini}\rangle \qquad (2.10)$$

with $\phi_k(\lambda)$ some basis functions for the smooth modification of the initial guess. Using Eq. (2.6), we obtain a linear system of equations for the coefficients α_k of the modification model, written in a K–vector $\boldsymbol{\alpha}$,

$$\mathbf{p}_\parallel = \mathbf{M} \cdot \boldsymbol{\alpha}. \qquad (2.11)$$

The elements of the matrix $\mathbf{M}$ are given by

$$M_{n,m} = \langle\, \phi_m\, p_{ini} \,|\, \varphi_n \,\rangle. \qquad (2.12)$$

For the K basis functions of the modification model, polynomials may be sufficient for simple passband shapes. For more complex passband shapes, where more freedom in modifying the initial guess may be desirable, B-spline basis functions may provide a convenient choice for the $\{\phi_k(\lambda)\}_{k=0,...,K-1}$.

3. Examples from HIPPARCOS

To illustrate the effect of the unconstrained orthogonal component of the passband, we take as an example three different passband solutions for the HIPPARCOS passband, H_p, derived by Weiler *et al.* (2018). These three possible solutions for H_p were obtained using the Next Generation Spectral Library (NGSL, Heap & Lindler (2016)) as calibration spectra, and they only differ in their orthogonal component with respect to the calibration
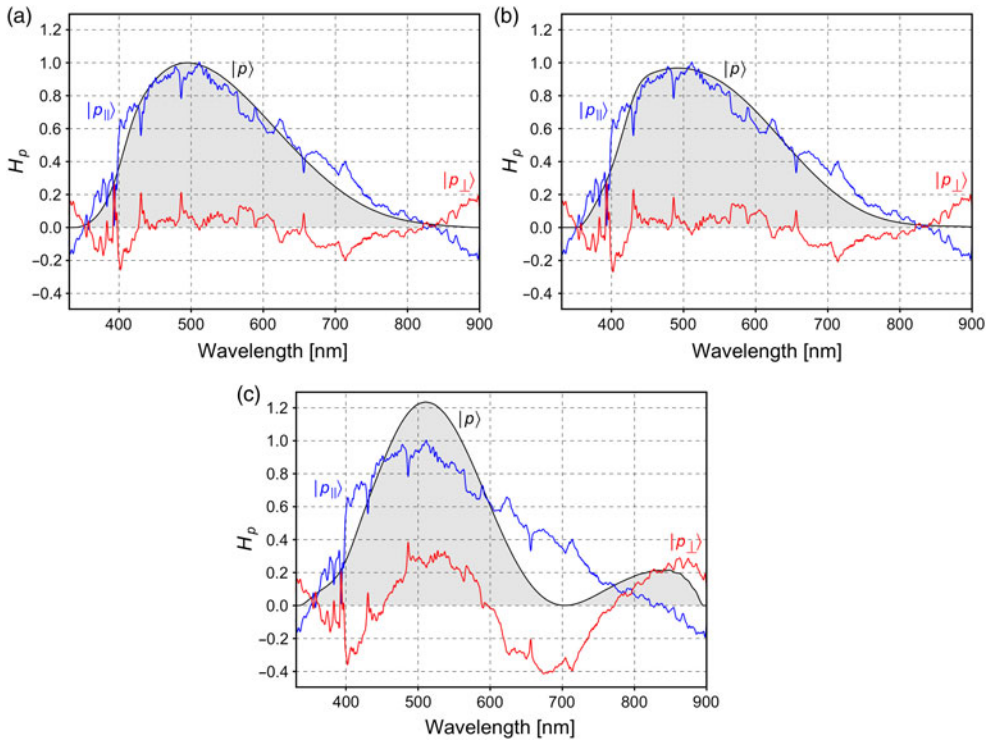
Figure 2. Three different solutions for the HIPPARCOS passband, which only differ in their orthogonal component (red lines), while the parallel component with respect to the calibration sources is kept fixed (blue lines). All passbands are normalised to the maximum of solution A.

spectra. The passbands, labeled A, B, and C, are shown in Fig 2. For each passband, the two components $|p_{\parallel}\rangle$ and $|p_{\perp}\rangle$ are provided, together with their sum $|p\rangle = |p_{\parallel}\rangle + |p_{\perp}\rangle$. While the solution A for H_p is the nominal solution from Weiler *et al.* (2018), solution B has been chosen to differ only slightly from A, while solution C has been deliberately chosen to be strongly different from any a-priori expectation for H_p. As $|p_{\parallel}\rangle$ is the same for all three solutions, they result in the same synthetic photometry for all calibration spectra used. However, the differences in $|p_{\perp}\rangle$ result in different synthetic photometry for sources whose SPDs are not well represented by a linear combination of the calibration SPDs.

To illustrate this effect, we take the empirical spectral library of Pickles (1998) and compute the synthetic HIPPARCOS magnitudes for the three different solutions. The difference between the synthetic magnitudes for solutions B and C with respect to solution A are shown in Fig. 3. The difference between the synthetic magnitudes from solution A and B (triangles in Fig. 3) is small, up to 57 mmag only. The differences however occur for sources with a large angle γ, which are the M-type spectra in the data set by Pickles (1998). Spectra of M-type sources are not included in the set of calibration sources, and these spectra are significantly different from the spectra included in the calibration set, in the sense that they are not linear combinations of the latter. The result is a large value for γ, and a strong dependency on the choice for $|p_{\perp}\rangle$. This effect is extreme for the difference between solution A and C. Although solution C results in essentially the same synthetic magnitudes for the Pickles spectra that are linear combinations of the NGSL calibration spectra (the sources with low values of γ), the differences for the M-type sources become extremely large, up to about 0.9 magnitudes. While this extreme case may be excluded
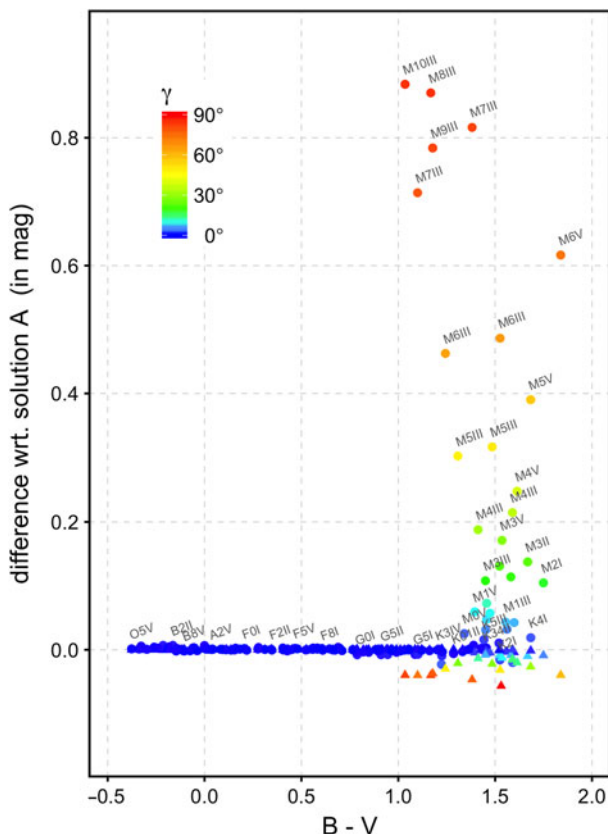
Figure 3. Difference between H_p solution B and A (triangles) and C and A (dots) for the spectra by Pickles (1998). The colour scale is indicating the γ angle according to Eq. (2.9). Selected spectral types are indicated.

in practice from the a-priori knowledge of the passband, less dramatic differences like the one between solution A and B may not be decided based on the available knowledge on how the passband should look like. Thus, systematic differences between the observed and synthetic magnitudes may result for sources not fully included by the vector space spanned by the calibration sources.

4. Summary and discussion

It has been demonstrated that deriving a passband from photometric observations of calibration sources with known SPDs is fundamentally limited by the choice of the calibration sources. A passband can be expressed as the sum of two functions. One of these functions, the "parallel component" of the passband, is a linear combination of the SPDs of the calibration sources and thus, up to uncertainties introduced by noise, uniquely determined by the calibration sources. The second function, the "orthogonal component" of the passband, is not contributing to the synthetic photometry of any of the calibration sources, and is in consequence unconstrained by the calibration spectra. The passband itself, i.e. the sum of the parallel and orthogonal component, is therefore not uniquely defined by any set of calibration spectra. A guess for the orthogonal component can be made based on any a-priori knowledge on the shape of the passband. Such guess however is intrinsically affected by uncertainties. While the synthetic photometry for SPDs which are a linear combination of the calibration SPDs only depends on the parallel passband

component, and therefore being reliable, SPDs which are not well represented by a linear combination of the calibration SPDs may not result in a reliable synthetic photometry. In the latter case, the synthetic photometry depends on the unconstrained orthogonal component, and the more so the less well the SPD is represented by a linear combination of the calibration SPDs.

Currently available libraries of calibration spectra, such as CALSPEC (Bohlin 2007) or Stritzinger *et al.* (2005), have been compiled mainly for the calibration of spectrophotometric data. They therefore exhibit a rather limited range of different spectral shapes, being dominated by hot sources. As a consequence, the space spanned by linear combinations of these calibration SPDs is rather limited as well, leaving many SPDs poorly covered. Among the objects with poorly covered SPDs are M-type stars, strongly extinct stellar objects, or largely non-stellar spectra, e.g. those of quasi-stellar objects. The limitation resulting from the limited coverage of spectral shapes among calibration libraries therefore prevents reliable synthetic photometry for many scientifically interesting objects. The set of calibration sources which is produced for the photometric and spectrophotometric calibration of ESA's *Gaia* mission (Gaia Collaboration *et al.* 2016) is improving in covering different shapes of SPDs, including objects from O to early M type (Pancino *et al.* 2012). A recent work by Maíz Apellániz & Weiler (2018) however has demonstrated the remaining limitation by the orthogonal passband component for M-dwarfs in the *Gaia* Data Release 2 passbands. A stronger diversification of spectral shapes in calibration libraries, aiming for a larger space spanned by linear combinations of their SPDs, may therefore be desirable for improving the interpretation of photometric data.

References

Bohlin, R. C. 2007, *Astronomical Society of the Pacific Conference Series*, 364, 315

ESA 1997, *The Hipparcos and Tycho Catalogues*, ESA-SP 1200

Gaia Collaboration, Prusti *et al.* 2016, *A&A*, 595, A1

Heap, S. R., and Lindler, D. 2016, *ASP Conference Series*, 503

Maíz Apellániz, J., & Weiler, M. 2018, *A&A*, in press

Pancino, E., Altavilla, G., Marinoni, S., *et al.* 2012, *MNRAS*, 426, 1767

Pickles, A. J. 1998, *PASP*, 110, 863

Stritzinger, M., Suntzeff, N. B., Hamuy, M., *et al.* 2005, *PASP*, 117, 810

Weiler, M., Jordi, C., Fabricius, C., & Carrasco, J. M. 2018, *A&A*, 615, A24

Weiler, M. 2018, *A&A*, 617, A138

Young, A. T. 1994, *A&A*, 288, 683